Imaging

9

Benedicte Lange and Karen-Lisbeth Bay Dirksen

Contents

B. Lange, MD (✉)
Department of Radiology,
University Hospitals of Aalborg, Aalborg, Denmark
e-mail: bl@benedictelange.dk

K.-L.B. Dirksen, MD
Department of Radiology,
University Hospital of Hillerød, Hillerød, Denmark

9.1 Summary

Imaging plays a central role in the diagnosis and treatment of distal radius fractures. Conventional radiography in 2 planes is still considered first choice imaging for wrist injuries. Image quality and a systematic diagnostic approach are however essential. Computer tomography (CT) is indicated in cases of uncertain radiograph findings and in comminuted, complex or intra-articular fractures and occasionally for presurgery assessment. Magnetic resonance imaging (MRI) is useful in assessment of tissue lesions and suspicion of fracture despite normal radiograph. Ultrasound is not considered routine modality in radius fracture diagnosis.

9.2 Introduction

Wrist traumas are amongst the most common injuries in the emergency department with fracture of the distal radius reported to be the most common upper extremity fracture (Larsen and Lauritsen 1993). There are few prospective, randomized trials to support different diagnostic strategies. Since wrist injuries are often complex comprising not only fractures but also a continuum of soft-tissue damages, great demands are put on a judicious imaging

L.M. Hove et al. (eds.), *Distal Radius Fractures*,
DOI 10.1007/978-3-642-54604-4_9,

Fig. 9.1 Imaging strategy

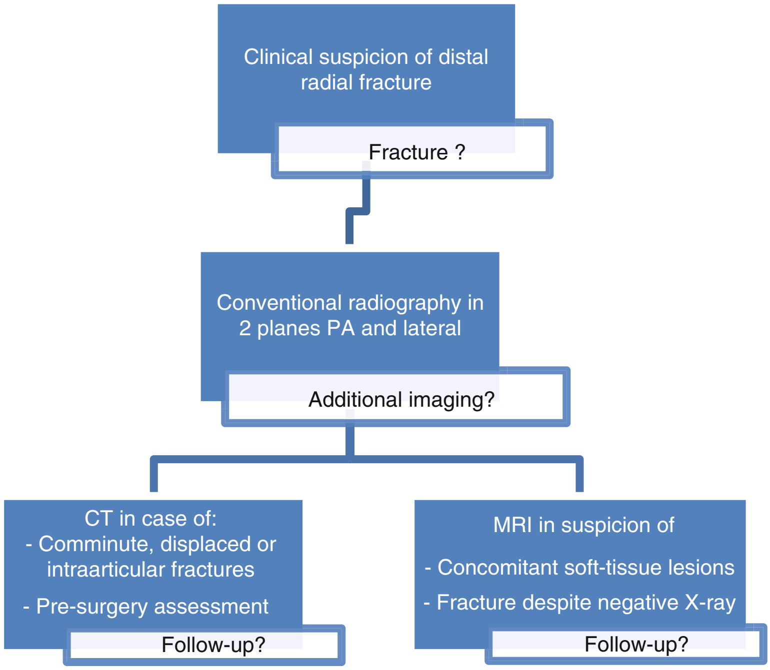

strategy, ensuring they are developed in close cooperation between the clinician and the radiologist (Fig. 9.1). This strategy should include immediate as well as possible follow-up imaging. Conventional radiography in at least 2 planes is still considered first choice imaging. In cases of uncertain radiograph findings, comminuted, displaced or intra-articular fractures or for presurgery assessment, computer tomography (CT) is the modality of choice (Trumble et al. 1999; Arora et al. 2010; Harness et al. 2006). Magnetic resonance imaging (MRI) is useful in the assessment of soft-tissue lesions and fracture suspicion despite negative radiograph (Goldfarb et al. 2011; Metz and Gilula 1993; Larsen et al. 1993). Ultrasound is not routine modality; however, it can be considered in an austere environment (McNeil et al. 2009) (Fig. 9.1).

9.3 Conventional Radiography

Wrist radiographs, which include the distal radius, distal ulna, carpal bones and metacarpal bases, can be a challenge. The 15 bones have subtle relationships that change with wrist positioning, which is why the adequacy of the radiograph is of utmost importance. The standard wrist series includes a posterior-anterior (PA – with shoulder in 90° abduction and elbow in 90° flexion) (Fig. 9.2) and lateral view (Fig. 9.3); more views can be added (Goldfarb et al. 2011).

First: Check the adequacy of the radiograph, the alignment and angles of the bones and the bone shapes (Table 9.1).

Second: Carefully evaluate and describe the radiograph systematically. Distal radial fractures are normally not difficult to identify but since they often are accompanied by soft

Fig. 9.2 PA view; should profile the extensor carpi ulnaris tendon groove, which should be at the level of or radial to the base of the ulnar styloid (*arrow*)

Fig. 9.3 Lateral view; the volar cortex of the pisiform bone (*1*) should overlie the central third of the interval between the volar cortices of the distal scaphoid pole (*2*) and the head of the capitate bone (*3*)

A meticulous 3-step approach to radiograph interpretation can be taken.

Tips and tricks –3-step approach for reading the radiograph

1. *Check adequacy, alignment and angles – see table 9.1*
2. *Evaluate and describe systematically – see table 9.2*
3. *Diagnose and decide treatment – see table 9.3*

tissue injuries resulting in dislocations of carpal bones, careful examination of all the structures in the wrist is necessary (Spence et al. 1998; Geissler et al. 1996) (see Table 9.2). Examples of fractures are displayed in Fig. 9.7.

Third: Diagnose and decide treatment. The classification of fractures is described elsewhere in this book. Table 9.3 displays how injuries are best viewed and Fig. 9.7 displays examples.

Table 9.1 Systematic assessment of the wrist radiograph

Adequacy of the radiograph	Alignment and angles of bones	Bony shapes
Distal 5 cm of radius to carpal-metacarpal junction is included	The three smooth articulating lines of the carpals are visible in PA view (Fig. 9.4)	*PA view* (Fig. 9.4)
Hand neutral in both the PA and lateral views. The axis of the middle metacarpal lines up with the middle of the radius (Figs. 9.2 and 9.3)	No more than 2–3 mm between individual carpal bones (Fig. 9.4)	The scaphoid should be “boat” shaped (scaphos is Greek for boat); a cortical ring implies displacement (signet-ring sign)
PA view	The radius articulates with at least half the lunate (Fig. 9.4)	The lunate should be quadrangular; a triangular shape implies rotation or displacement
Should profile the extensor carpi ulnaris tendon groove, which should be at the level of or radial to the base of the ulnar styloid (Fig. 9.2)	Articular surface of ulna at the same height or slightly shorter as the articular surface of radius (shorter ulna, ulna minus; longer ulna, ulna plus)	The pisiform is the last carpal to ossify up to age 12 years
Lateral view	*PA view* (Fig. 9.5)	
The palmar cortex of the pisiform bone should overlie the central third of the interval between the palmar cortices of the distal scaphoid pole and the capitate head (Fig. 9.3)	Radial inclination 21–25° Radial height 10–13 mm *Lateral view* (Figs. 9.4 and 9.5) Radial volar tilt 0–22° (average 11°) Scapholunate (SL) angle 30–60° Capitolunate (CL) angle < 30°	

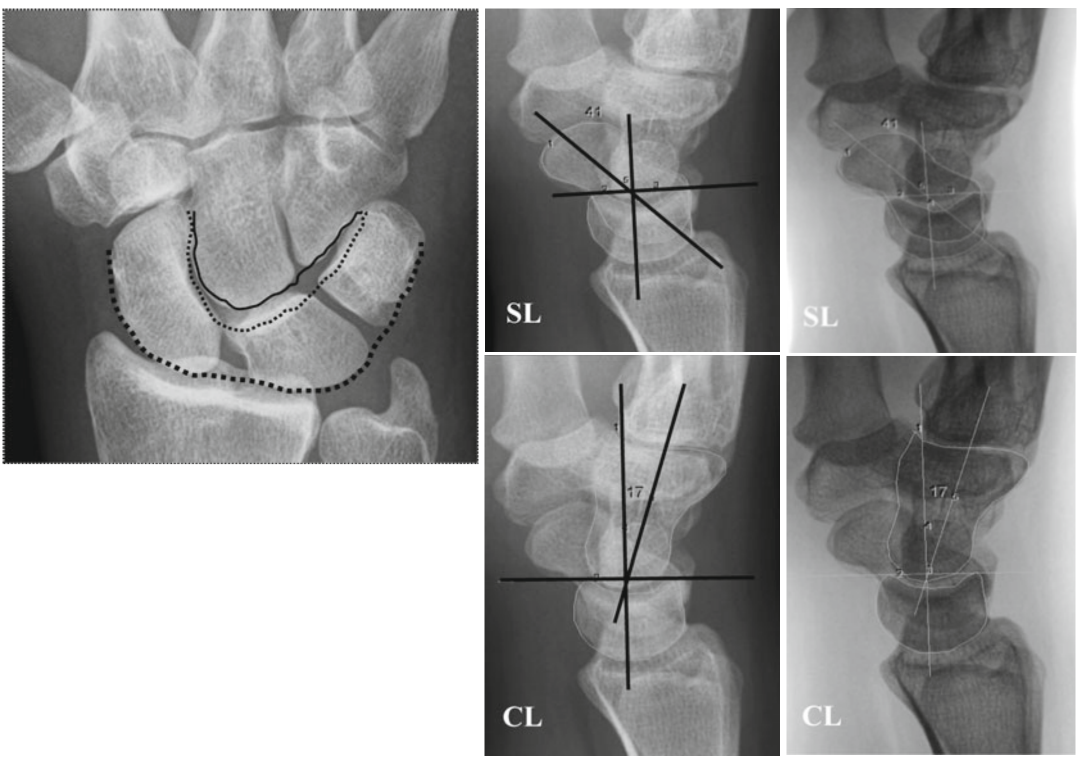

Table 9.2 Evaluation and description of findings on the radiograph

Evaluation and description of pathological findings on the radiograph
Check both PA and lateral views!
Look for:
Soft tissue swelling – observe underlying cortices
Bone cortices discontinuity:
PA: cortices of scaphoid, lunate and distal radius
Lateral: all cortical structures (distal radius, ulna, carpal bones, metacarpal cortices)
Articular surface discontinuity
Distance between carpals – carpal instability
Scapholunate instability:
Distance between scaphoid and lunate > 3 mm (Terry-Thomas sign)
PA view: abnormal angle of the scaphoid (signet-ring sign)
Lateral view (Fig. 9.6): scapholunate angle can be increased (dorsal scapholunate instability, DISI) or decreased (volar scapholunate instability, VISI)
Perilunate dislocation (severe, seldom, requires forced injury to the wrist) – distal carpal row dislocates dorsal together with the capitate in relation to the lunate
Describe the fracture:
Simple or compound
Transverse, oblique or spiral
Comminute
Complex
Impacted
Dislocation
Avulsion
Fissure
Greenstick
Measure:
Radial height
Radial angle
Note other findings:
Osteoporosis
Osteoarthritis
Arthritis
Other abnormal findings

Fig. 9.4 Normal wrist radiograph: three smooth articulating lines of the carpals are visible, there is no more than 2–3 mm between individual carpal bones and the radius articulates with at least half the lunate. The scaholunate angle (*SL*) is measured by drawing a line through or parallel to the long axis of the scaphoid bone (*5*), then a helping line parallel to the articular surface of the lunate (*3*) and then a line perpendicular to the articular distal surface of the lunate (*4*). The SL angle is measured between line 4 and 5 and should normally be 30–60° (in this example it is 41°). 1 and 2 represents the outlines of the scaphoid and the lunate. The capitolunate angle (*CL*) is measured by drawing a line through the longitudinal axis of the capitate (*5*), then a helping line parallel to the articular surface of the lunate (*3*) and then a line perpendicular to the articular distal surface of the lunate (*4*). The CL angle is measured between line 4 and 5 and is normally < 30° (in this example 17 °). 1 and 2 represents the outline of the capitate and the lunate

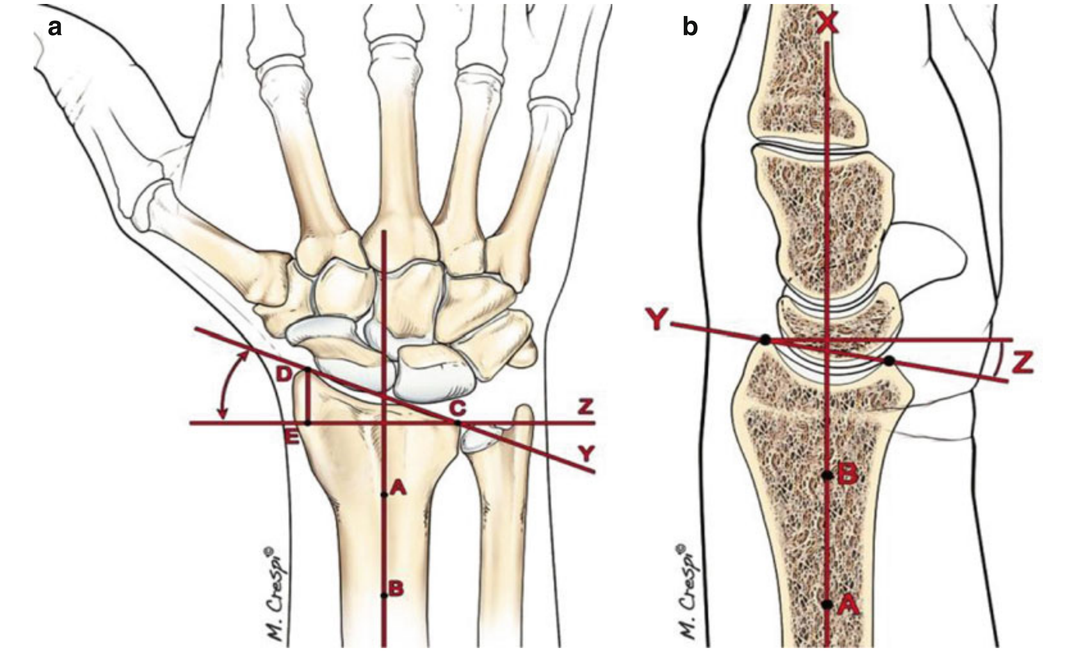

Fig. 9.5 Measurement of radial inclination and radial volar tilt. (**a**) Radial inclination angle (*arrow*) is measured by drawing a perpendicular line (line *EC*) to the radial axis (*AB*) through the ulnar edge of the lunate fossa and another line (line *DC*) joining the distal tip of the radial styloid and the ulnar edge of the lunate fossa. These two lines form the radial inclination angle (normal angle, 21–25°). Radial height is the measured distance between points *D* and *E*, where *D* represents the distal-most tip of the radial styloid and *E* is a point on line *EC*. Line *DE* is the shortest distance between point *D* and line *EC*. Normal radial height is 10–13 mm. (**b**) The palmar (volar) tilt is the angle created between the line (*Y*) joining the most distal points of the dorsal and ventral rims of the distal articular surface of the radius and the line (*Z*) drawn perpendicular to the long axis (line *XBA*) of the radius. The average tilt is 11°, with a range of 0–20°

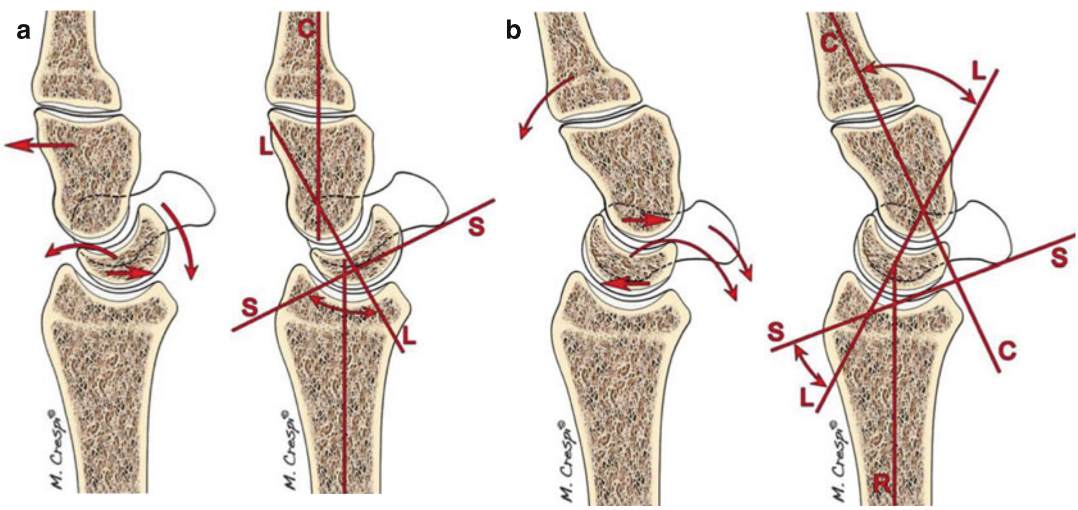

Fig. 9.6 (**a**) Dorsal scapholunate instability – (DISI). *SL* angle is increased. (**b**) Volar scapholunate instability – (VISI). *SL* angle is decreased. *S* line along the base or center of the scaphoid, *L* line perpendicular to the lunate, *C* line along the long axis of the capitate, *R* line along the long axis of the radius, *S–L* lines form the scapholunate angle (SL), *C-L* lines form the capitolunate angle (CL)

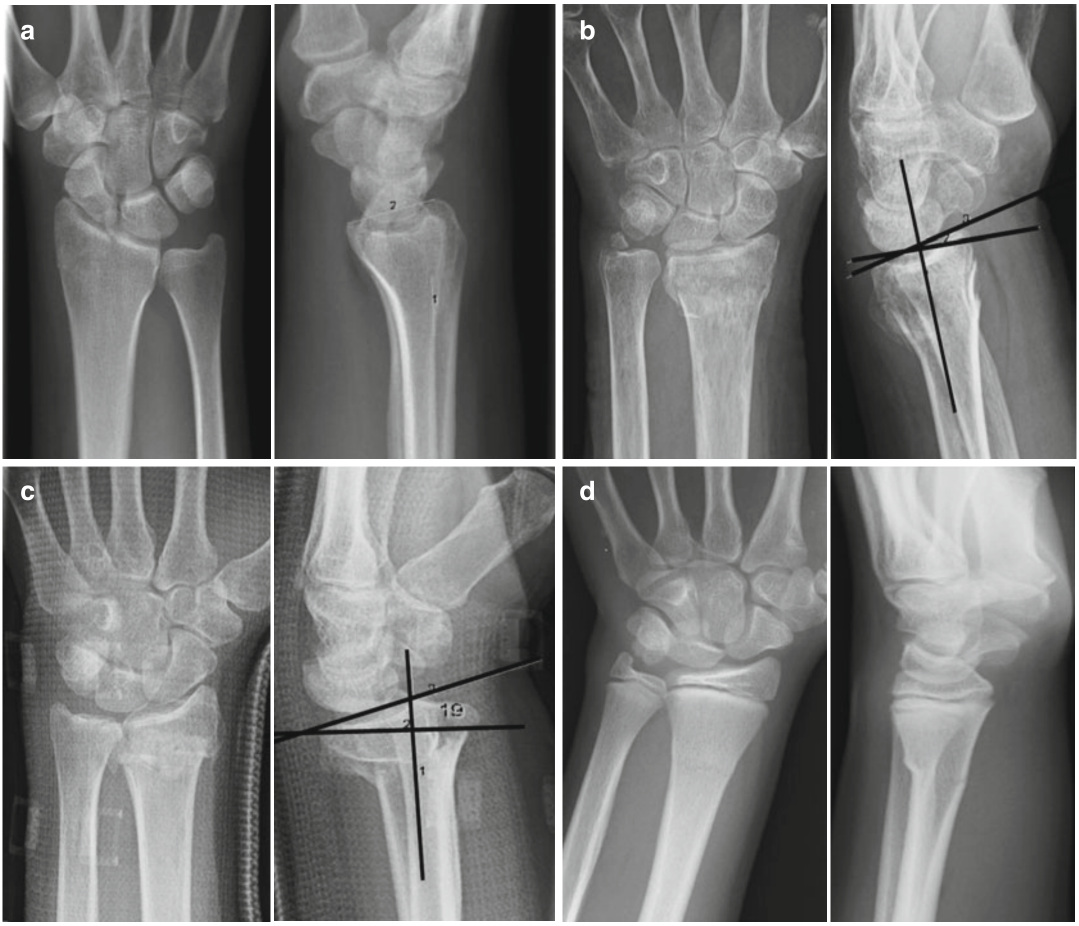

Fig. 9.7 Examples of common fractures and injuries. (**a**) Intra-articular fracture of the radial styloid. (**b**) Smith's fracture with a volar tilt. (**c**) Colles fracture with dorsal tilt of distal fragment. (**d**) Greenstick fracture of distal radius. The lines (1, 2, 3 and 19) drawn at the lateral radiographs show how to measure the tilt of the articular surface of the radius according to Fig. 9.5

9.4 Computer Tomography (CT) Scanning

As mentioned, conventional radiography is usually sufficient for correct diagnosis and adequate treatment of distal radius fractures. CT scans provide more accurate information regarding the anatomy of intra-articular fractures than radiography, and 70–81 % distal radius fractures have been reported to have intra-articular extension. Healing with residual incongruity of 2 mm or more carry a risk of almost 100 % of developing secondary radiographic visible osteoarthritis. The addition of CT to plain films frequently changes the therapeutic recommendations for such cases, and CT is also valuable in case of comminute fractures and before surgery (Trumble et al. 1999; Arora et al. 2010; Harness et al. 2006; Slutsky 2013).

A CT scanner emits a series of narrow beams through an arc moving spirally 360° around the body. A 64-slice CT scanner has 64 rows of 0.625 mm slices giving a 40 mm detector width, which transmits the collected data to a computer, from which 2D and 3D images in high resolution are reconstructed. The patient is placed supine with the arm stretched over the head and the wrist angled a little to the central beam to avoid artefacts (Fig. 9.8). CT scan examples are displayed in Figs. 9.9 and 9.10.

Promising results regarding demonstration of instability between the carpal bones have been shown using dynamic CT scans; however,

Table 9.3 Views best suitable for diagnoses

Views	Diagnoses
PA	Colles or Smith's fracture (transverse fracture of distal radius with dorsal or volar tilt of distal fragment associated with avulsion of ulnar styloid)
	Radial styloid/Chauffeur/Hutchinson fracture (oblique, intra-articular fracture of the radial styloid which may be associated with intercarpal ligamentous injuries, especially of the scapholunate ligament)
	Galeazzi fracture (distal 1/3 of the diaphysis of the radius associated with luxation of the distal radioulnar joint)
	Essex-Lopresti fracture (fracture of radial head and/or luxation of the proximal radioulnar joint associated with rupture of interosseous membrane with dislocation of distal radioulnar joint)
	Ulnar variance (plus/minus)
	Distal radial ulnar joint (DRUJ) injury
	Perilunate dislocation
	Scapholunate or other ligament lesions
Lateral	Colles fracture (transverse fracture of the distal radius with dorsal tilt of distal fragment associated with avulsion of ulnar styloid)
	Smith's fracture (a reversed Colles fracture with volar tilt of the distal fracture fragment)
	Barton's fracture (comminuted fracture of the distal articular surface + volar or dorsal subluxation of fragment and carpus)
	Galeazzi fracture (distal 1/3 of the diaphysis of the radius associated with luxation of the distal radioulnar joint)
	Essex-Lopresti fracture (fracture of radial head and/or luxation of the proximal radioulnar joint associated with rupture of interosseous membrane with dislocation of distal radioulnar joint)
	(Radio-)carpal subluxations
	Ligament lesions between the carpals

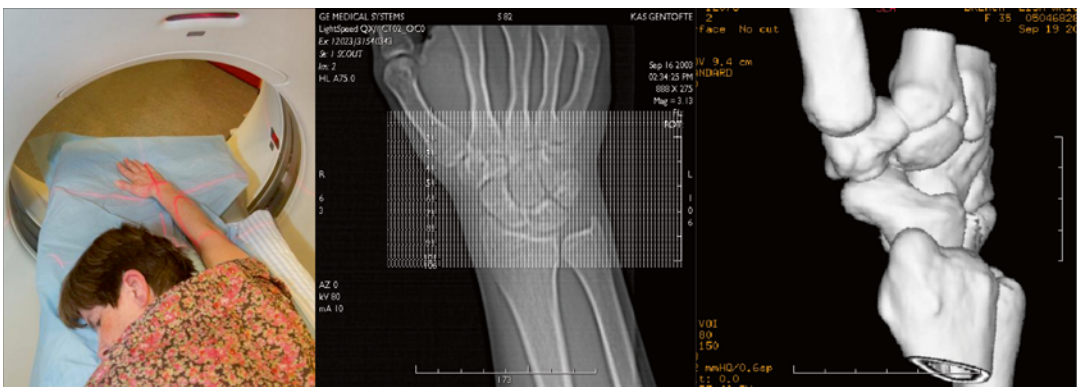

Fig. 9.8 CT scan in 3 planes with reconstruction

more studies are needed (Kalia et al. 2009; Leng et al. 2011).

9.5 Magnetic Resonance Imaging (MRI)

MRI is the modality of choice for visualization of soft-tissue injuries and hidden fractures of the wrist (Fotiadou et al. 2011). The MRI technique is entirely different from conventional radiography and CT scanning, not creating images based upon high-energy electromagnetic waves (X-rays), but upon magnetic and radio waves. The patient lies inside a large, cylinder-shaped magnet, the strength of which is measured in tesla, which is 10,000–30,000 times stronger than the magnetic field of the earth. This strong magnetic field causes alignment of the positively charged body hydrogen protons, themselves acting like small

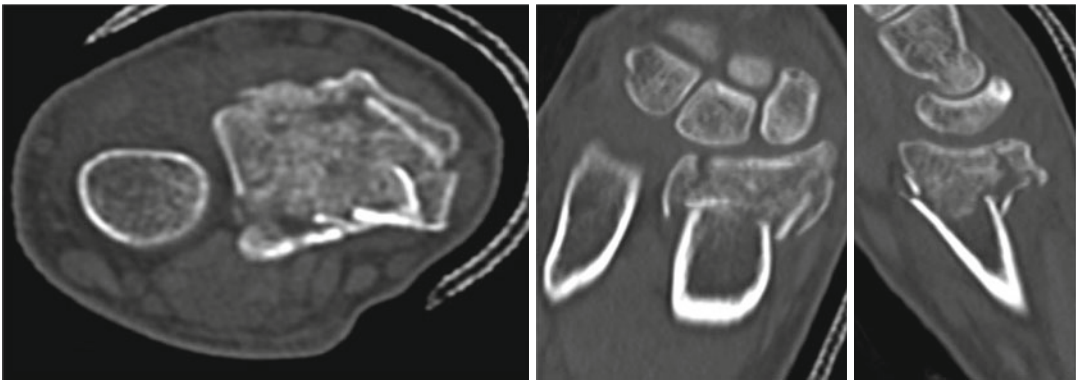

Fig. 9.9 CT scan in axial, coronal and sagittal plane

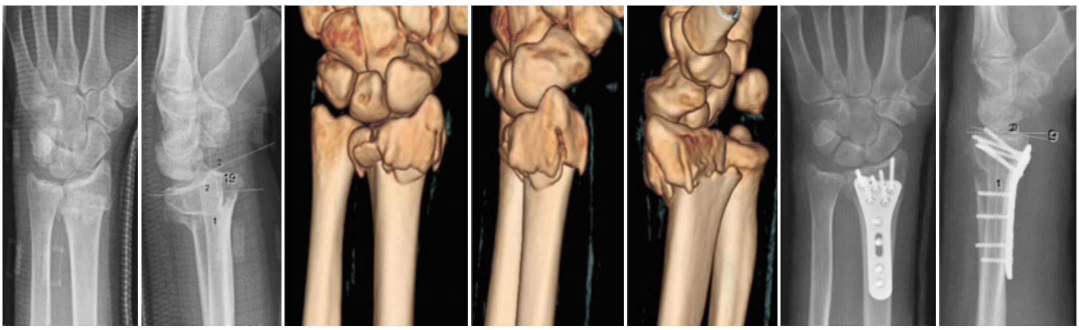

Fig. 9.10 Comminuted distal intra-articular radial fracture with dorsal tilt: conventional radiograph, preoperative 3D CT scan and postoperative control radiograph. The lines (1, 2, 3, 9, and 19) at the lateral radiograhps shows the tilt of the articular surface before and after operation according to Fig. 9.5

magnets. Radio waves are then sent through the body causing disturbance of this alignment. When the waves are switched off again, the hydrogen protons spin back to their original aligned position, projecting radio waves of their own. The scanner receives these signals, and a computer turns them into pictures in axial, coronal and sagittal planes. Since the signals are tiny, the wrist is placed in a coil (antenna). By changing the timing of the radio wave pulses, it is possible to gain information about the different types of tissue. Since movable hydrogen protons are mainly found in fat, water and soft tissue, these structures will project the strongest signals, which appear white on the MRI picture. Low signals, such as calcified bones, appear dark. Depending on when the radio waves are turned off, different signals, the so-called sequences, are developed.

It can now be understood why MRI is of benefit in cases of suspected concomitant ligamentous injuries or fractures not demonstrated on routine radiographs, since the MRI will visualize soft tissue and oedema. The ligamentous elements are important for the stabilization of the wrist. They dictate much of the injury pattern and account for many missed wrist injuries seen in association with distal radius fractures (Larsen et al. 1993). It has been reported that 68 % of patients requiring operative repair of a radius fracture had injuries to the soft tissues, including the triangular fibrocartilage complex and the scapholunate or the lunate-triquetral ligaments (Geissler et al. 1996). Arthrography is valuable when looking for such defects (Goldfarb et al. 2011). MRI is also valuable for follow-up in case of persistent discomfort after injury (Fotiadou et al. 2011).

The MRI is considered harmless to the patient as opposed to conventional radiographs and CT scans; however, they are costly, time consuming and challenging for patients suffering from claustrophobia. The cost-benefit of additional MRI is still under debate (Nikken et al. 2005).

The sequences used for imaging of the wrist are called T1, T2, STIR (short tau inversion recovery) and T2 with fat suppression, and opposed to CT, reconstruction is not possible; the sequences have to be chosen before the examination. Table 9.4 illustrates which types of tissue give high and low signals in the different sequences. For strengths and weaknesses of the different sequences, see Table 9.5. Examples of soft-tissue injuries are displayed in Fig. 9.11.

Table 9.5 Strengths and weaknesses of MRI sequences

Sequence	Strengths	Weaknesses
T1	Anatomy Fat tissue Meniscus Contrast enhancement	Oedema
T2	Oedema Pathological processes	Movement sensitive
STIR or T2 fat suppressed	Oedema Pathological processes	Not as good as T2 for details

Tips and tricks – difficult to remember in which sequences water is white?

STIR WHITE WATER IN THE TEA TOO!!
(Water is white in STIR and T2)

Table 9.4 Water and fat signals in different MRI sequences – insufficient healing of radial styloid fracture

	T1	T2	STIR or T2 fat suppressed
Water signal	Black	White	White
Fat signal	White	Grey/white	Black
			

Fig. 9.11 Examples of soft tissue and bone injuries on MRI. (**a**) Lesion of the triangular fibrocartilage discus with water signal in the distal radioulnar joint. (**b**) Scaphoid fracture: sagittal CT and MRI T1 and STIR

9.6 Ultrasound

Ultrasound is not considered to be routine modality in the diagnosis of wrist injuries. It has been shown that the use of ultrasound by an experienced clinician in an austere environment can be performed accurately and may possibly prevent unnecessary evacuations for suspected fractures requiring radiographic verification (McNeil et al. 2009).

References

Arora S, Grover SB, Batra S, Sharma VK. Comparative evaluation of postreduction intra-articular distal radial fractures by radiographs and multidetector computed tomography. J Bone Joint Surg Am. 2010; 92(15):2523–32.

Fotiadou A, Patel A, Morgan T, Karantanas AH. Wrist injuries in young adults: the diagnostic impact of CT and MRI. Eur J Radiol. 2011;77(2):235–9.

Geissler WB, Freeland AE, Savoie FH, McIntyre LW, Whipple TL. Intracarpal soft-tissue lesions associated with an intra-articular fracture of the distal end of the radius. J Bone Joint Surg Am. 1996;78(3):357–65.

Goldfarb CA, Yin Y, Louis AG, Fisher AJ, Boyer MI. Wrist fractures: what the clinician wants to know. Radiology. 2011;219:11–28.

Harness NG, Ring D, Zurakowski D, Harris GJ, Jupiter JB. The influence of three-dimensional computed tomography reconstructions on the characterization and treatment of distal radial fractures. J Bone Joint Surg Am. 2006;88(6):1315–23.

Kalia V, Obray RW, Filice R, Fayad LM, Murphy K, Carrino JA. Functional joint imaging using 256-MDCT: technical feasibility. Am J Radiol. 2009;192(6):w295–9.

Larsen CF, Lauritsen J. Epidemiology of acute wrist trauma. Int J Epidemiol. 1993;22(5):911–6.

Larsen CF, Brondum V, Wienholtz G. An algorithm for acute wrist trauma. A systematic approach to diagnosis. J Hand Surg Br. 1993;18(2):207–12.

Leng S, Zhao K, Qu M, An K, Berger RA, McCollough CH. Dynamic CT technique for assessment of wrist joint instabilities. Med Phys. 2011;38(7):50–6.

McNeil CR, McManus J, Mehta S. The accuracy of portable ultrasonography to diagnose fractures in austere environment. Prehosp Emerg Care. 2009;13: 50–2.

Metz VM, Gilula LA. Imaging techniques for distal radius fractures and related injuries. Orthop Clin North Am. 1993;24(2):217–28.

Nikken JJ, Oei EH, Ginai AZ, Krestin GP, Verhaar JA, van Vugt AB, et al. Acute peripheral joint injury: cost and effectiveness of low-field-strength MR imaging–

results of randomized controlled trial. Radiology. 2005;236(3):958–67.
Slutsky D. Predicting the outcome of distal radius fractures. Hand Clin. 2013;21(2005):289–94.
Spence LD, Savenor A, Nwachuku I, Tilsley J, Eustace S. MRI of fractures of the distal radius: comparison with conventional radiographs. Skeletal Radiol. 1998; 27(5):244–9.
Trumble TE, Culp RW, Hanel DP, Geissler WB, Berger RA. Intra-articular fractures of the distal aspect of the radius. Instr Course Lect. 1999;48:465–80.